Multimodal Fundus Imaging of Sodium Iodate-Treated Mice Informs RPE Susceptibility and Origins of Increased Fundus Autofluorescence

Jin Zhao,[1] Hye Jin Kim,[1] and Janet R. Sparrow[1,2]

[1]Department of Ophthalmology, Columbia University Medical Center, New York, New York, United States
[2]Pathology and Cell Biology, Columbia University Medical Center, New York, New York, United States

Correspondence: Janet R. Sparrow, Department of Ophthalmology, Columbia University Medical Center, 635 W. 165th Street, New York, NY 10032, USA; jrs88@cumc.columbia.edu.

Submitted: January 25, 2017
Accepted: March 15, 2017

Citation: Zhao J, Kim HJ, Sparrow JR. Multimodal fundus imaging of sodium iodate-treated mice informs RPE susceptibility and origins of increased fundus autofluorescence. *Invest Ophthalmol Vis Sci*. 2017;58:2152–2159. DOI:10.1167/iovs.17-21557

Purpose. By multimodal imaging, and the use of mouse and in vitro models, we have addressed changes in fundus autofluorescence (488 and 790 nm) and observed interactions between the photooxidative stress imposed by RPE bisretinoid lipofuscin and the oxidative impact of systemic sodium iodate ($NaIO_3$).

Methods. *Abca4*$^{-/-}$, wild-type, and *Rpe65*^{rd12} mice were given systemic injections of $NaIO_3$ (30 mg/kg). Analysis included noninvasive imaging of fundus autofluorescence (short-wavelength [SW-AF]; near-infrared excitation [NIR-AF]), quantitative fundus AF (qAF; 488 nm); light microscopy, RPE flat-mounts and measurements of outer nuclear layer (ONL) thickness. $NaIO_3$ also was studied by using in vitro assays.

Results. In SW-AF and NIR-AF images, fundus mottling was visible 3 and 7 days after $NaIO_3$ injection with changes being more pronounced in *Abca4*$^{-/-}$ mice that are characterized by an abundance of RPE bisretinoid lipofuscin. In *Abca4*$^{-/-}$ mice, qAF was elevated 3 and 7 days after $NaIO_3$ administration. In light micrographs and RPE flat-mounts stained to reveal tight junctions (ZO-1) and nuclei, the RPE monolayer was disorganized, and clumping and loss of RPE was visible. ONL thinning was most pronounced in *Abca4*$^{-/-}$ mice. Treatment of ARPE-19 cells with $NaIO_3$ together with the photooxidation of the bisretinoid A2E by exposure to 430-nm light produced an additive effect whereby loss of cell viability was greater than with either perturbation alone.

Conclusions. Elevations in SW-AF intensity can occur due to photoreceptor cell dysfunction as induced secondarily by $NaIO_3$. Photooxidative stress associated with RPE cell bisretinoid lipofuscin may confer increased susceptibility to the oxidant $NaIO_3$.

Keywords: bisretinoid, lipofuscin, retina, retinal pigment epithelium, sodium iodate

When delivered systemically, sodium iodate ($NaIO_3$), a strong oxidant, is known to primarily target RPE cells with effects on photoreceptor cells occurring secondarily.[1–6] In recent years, $NaIO_3$ administration in rats and mice has been used to model the atrophic lesions that are a feature of AMD[7] and has been favored as a means to denude RPE in advance of cell therapy.[4,5,8–10]

The structural changes resulting from $NaIO_3$ retinal damage have been extensively reported. Following a single injection of $NaIO_3$, degeneration begins with the RPE cell followed by loss of photoreceptor cell nuclei in subjacent outer nuclear layer (ONL).[11] The choriocapillaris underlying RPE also undergoes atrophy. Central retina is damaged preferentially.[11,12] The changes can be monitored by ERG, by measuring visual acuity (optomotor reflex) by light microscopy, TUNEL assay, and by quantifying lipid peroxidation products.[5,13–16]

Several mechanisms have been associated with $NaIO_3$-mediated damage[6,17–19] with the differences in pathways followed being dose-associated.[3,19] For instance, $NaIO_3$-stress activates the AKT/mammalian target of rapamycin (AKT/mTOR) signaling pathway in RPE, whereas rapamycin delivered to inhibit mTOR attenuates $NaIO_3$-associated retinal degeneration.[20] Observations made after delivering a low dose of $NaIO_3$ (20 mg/kg) to mice deficient in αB crystallin indicate that this small heat shock protein may provide protection against oxidative stress by upregulating AKT phosphorylation and peroxisome proliferator-activator receptor-γ expression.[3] $NaIO_3$ is known to directly oxidize thiol (-SH) groups resulting in an increase in the number of disulphide (S-S) bonds.[21] Moreover, cotreatment with cysteine or glutathione reduces the damage to RPE caused by $NaIO_3$.[22] When oxidative stress is induced with $NaIO_3$, an age-related increase in superoxide anion and malondialdehyde is observed.[13] It is also reported that murine and human RPE cells cultured in the presence of $NaIO_3$ are induced to generate reactive oxygen species.[3] Additionally, $NaIO_3$ is said to denature protein.[23]

Interactions between $NaIO_3$ and light also have been shown with the effects of $NaIO_3$ being greater in mice exposed to bright light.[24] The impact is also greater in albino mice and rats as opposed to pigmented rodents.[15] When the effects of $NaIO_3$ were compared in young (2 month) versus older (15 month) mice, age-associated effects were observed.[13]

$NaIO_3$ is an oxidizing agent due to its ability to extract electrons, but why the RPE is particularly susceptible to $NaIO_3$-induced damage is not clear. Besides the metabolic sources of oxidative stress, RPE cells are subject to photooxidative damage

originating in the bisretinoid fluorophores that form in photoreceptor cells and accumulate with age as the lipofuscin of RPE cells.[25] Short-wavelength fundus autofluorescence (SW-AF) originates primarily from these fluorophores in RPE. In some retinal disorders, such as acute macular neuroretinopathy and fundus flecks in Stargardt disease 1 (STGD1),[26,27] we have noted localized elevations in SW-AF and proposed that this aberrant SW-AF may be a sign that photoreceptor cells are incapacitated and thus unable to expend the energy necessary to reduce visual cycle–derived retinaldehyde to nontoxic retinol. Thus, our objective here has been 2-fold. First, we tested for whether bisretinoid formation is increased when photoreceptor degeneration is induced, in this case degeneration secondary to $NaIO_3$-associated RPE loss. We addressed this question by examining for evidence of enhanced SW-AF as measured by an established protocol (quantitative fundus autofluorescence [qAF]). The second question we addressed was whether RPE cells are susceptible to $NaIO_3$ because of preexisting stress imposed by the photooxidative processes initiated by RPE bisretinoids. To this end, we studied the effects of $NaIO_3$ administration in mice having elevated levels of bisretinoid lipofuscin (*Abca4*$^{-/-}$ mice),[28] wild-type levels of bisretinoid lipofuscin, and mice (*Rpe65*^{rd12}) that do not generate the visual cycle adducts constituting bisretinoid lipofuscin.[29,30]

Methods

Animals

Agouti 129S-Abca4tm1Ght/J mice and their control 129S1/SvImJ mice, as well as pigmented *Rpe65*^{rd12} mice were purchased from Jackson Laboratories (Bar Harbor, ME, USA) and bred in-house. All mice were housed under 12-hour on-off cyclic lighting with in-cage illuminance of approximately 40 lux. A sterile solution of $NaIO_3$ (Sigma-Aldrich Corp., St. Louis, MO, USA) was freshly prepared in PBS. $NaIO_3$ was administered as a single intraperitoneal injection (30 mg/kg body weight). Animal protocols were approved by the Institutional Animal Care and Use Committee of Columbia University and complied with guidelines set forth by the ARVO Animal Statement for the Use of Animals in Ophthalmic and Vision Research.

Fundus Imaging

Mice were anesthetized, pupils were dilated, the cornea was lubricated, and mice were positioned as previously described.[31] Fundus AF images (55° widefield lens; 0.98-mm detection pupil) at 488 nm and 790 nm excitation were obtained with a confocal scanning laser ophthalmoscope (Spectralis HRA; Heidelberg Engineering, Heidelberg, Germany) with laser power set at approximately 280 μW and sensitivity at 100 and 105, respectively, after visual pigment was bleached for 20 seconds. Nine successive frames were acquired at 488 nm excitation with the high-speed mode, and frames were saved in non-normalized mode. A mean of 100 frames was obtained at 790-nm excitation with high-resolution automatic real-time mode, and resized with Photoshop CS4 (Adobe Systems, Inc., San Jose, CA, USA) to 768 × 768 pixels, the same as high-speed mode images. Near-infrared reflectance images (NIR-R) (820 nm) were also acquired.

Quantitative Fundus Autofluorescence

Using a dedicated image analysis program written in IGOR (Wavemetrics, Lake Oswego, OR, USA), mean gray levels (GLs) were calculated from eight predefined segments around the optic disc and blood vessels were excluded by histogram analysis. qAF at 488-nm excitation was calculated by normalization to the GL of the reference after subtraction of zero light (GL_0) and inclusion of a reference calibration factor.[32,33] Fluorescence intensities at 790 nm were calculated by subtracting the minimal GL of optic nerve head measured by ImageJ software (http://imagej.nih.gov/ij/; provided in the public domain by the National Institutes of Health, Bethesda, MD, USA).

Histology

Mouse eyes were marked with a tissue dye and fixed in Alcoholic Z-fix (provided by Excalibur Pathology, Inc., Norman, OK, USA), and 5-μm hematoxylin and eosin–stained paraffin sections were prepared by Excalibur. The sections most centrally located within the optic nerve head (ONH) were imaged with an Axioskop2 microscope (Carl Zeiss, Jena, Germany) and recorded with a digital camera (ORCA100; Hamamatsu Photonics, Hamamatsu City, Japan) that was controlled by a MetaMorph image-processing program (Universal Imaging Co., Downingtown, PA, USA). Images were compiled in Photoshop CS4 and the levels command was used to adjust the contrast of all images simultaneously. ONL width was measured at 200-μm intervals and plotted as distance (mm) superior and inferior to the ONH in the vertical plane. ONL area was calculated by summing ONL thickness in superior and inferior hemiretina (ONH to 2.0 mm) and multiplying by the measurement interval of 0.2 mm.

Immunostained Flat-Mounts

Mouse eyes were enucleated and fixed in 2% paraformaldehyde in PBS for 2 hours at room temperature. After removing the cornea, lens, and neural retina, radial cuts were made to the posterior eyecup to flatten the sclera, choroid, and RPE onto a glass slide with RPE being uppermost. To inhibit nonspecific binding, the specimens were incubated in 10% donkey serum/0.2% saponin in PBS for 3 hours, and then in primary antibodies (rat anti-ZO-1, 1:20; DSHB Iowa, Iowa City, IA, USA; rat anti-F4/80, 1:100, eBioscience, San Diego, CA, USA) at room temperature overnight. After washing, the flat-mounts were incubated with donkey anti-rat secondary antibodies (Jackson ImmunoResearch Laboratories, West Grove, PA, USA) and counterstained with a nuclear dye DAPI (4′,6-diamidino-2-phenylindole; Sigma-Aldrich Corp., St. Louis, MO, USA). Fluorescent images were recorded with an Axioskop2 microscope (Carl Zeiss) and recorded with a digital camera (ORCA100) that was controlled by a MetaMorph image-processing program (Universal Imaging Co.). Images were compiled in Adobe Photoshop CS4 extended and the levels command was used to adjust the contrast of all images simultaneously.

Quantitative Ultra-Performance Liquid Chromatography (UPLC)

Analysis was performed on a Waters Acquity UPLC system (Waters Corp, Milford, MA, USA) coupled on-line with a photodiode array detector. For elution, a Waters XBridge C18 reversed-phase column (2.5 μm, 3 × 50 mm) was used with a mobile phase of acetonitrile/methanol (1:1) in water with 0.1% formic acid (0–1 minute, 70% acetonitrile/methanol [1:1] in water; 1–27 minutes, 98% acetonitrile/methanol [1:1] in water; 27–30 minutes, acetonitrile/methanol [1:1]; flow rate of 0.5 mL/min) and injection volume of 5 μL. A2E peak area was integrated from UPLC chromatograms by using Waters Empower software.

In Vitro Experiments

In an in vitro photooxidation assay, synthesized A2E (50 μM)[34] in 1% dimethyl sulfoxide (DMSO) in PBS without and with $NaIO_3$ (5–500 μM, as indicated) was irradiated (430 ± 30 nm, 60s), and quantified. In other experiments, A2E (50 μM) in PBS with 1% DMSO was incubated (room temperature in the dark) with $NaIO_3$ (100, 200 μM, as indicated) for 4 hours; controls were incubated without $NaIO_3$. To test for direct effects of $NaIO_3$ on cultured RPE, ARPE-19 cells (American Type Culture Collection, Manassas, VA, USA) deficient in endogenous lipofuscin[34] were grown to confluence in 96-well plates as described.[35] The cells accumulated A2E by delivery in culture media (3 μM) over 14 days. After culturing for an additional 5 days in media without A2E, the cells were incubated with $NaIO_3$ (25, 250 μM and 2.5 mM) for 24 hours and then exposed to 430-nm light (±30 nm, time) and after 18 hours, MTT (4,5-di-methylthiazol-2-yl)-2,5-diphenyltetrazolium bromide) assay (Roche Diagnostics, Indianapolis, IN, USA) was performed to evaluate cell viability.

Statistical Analysis

Statistical analysis was performed by using GraphPad Prism, version 6 (GraphPad Software, Inc., La Jolla, CA, USA); $P < 0.05$ was considered significant.

Results

The effects of $NaIO_3$ administration are well known to depend on the dose and route of administration.[3,5,36] In initial experiments, we injected mice intraperitoneally with $NaIO_3$ at concentrations of 30 and 60 mg/kg to determine an appropriate dose of intraperitoneal $NaIO_3$ that would be delivered by single injection. We selected the 30 mg/kg dose for all further experiments because it produced moderate degeneration that could be detected 7 days after injection in all injected mice.

Fundus Imaging

To evaluate the effects of a moderate dose of $NaIO_3$ on retina, we acquired fundus images of the *Abca4*$^{-/-}$, wild-type, and *Rpe65*^{rd12} mice (age 6 months) using the NIR-R (820 nm), SW-AF (488 nm), and NIR-AF (790 nm) modalities (Fig. 1A). Fundus AF generated by 488-nm excitation originates predominantly from the bisretinoids that accumulate in RPE as lipofuscin.[37] NIR-AF is emitted from melanin of RPE with a smaller contribution from choroid.[38] Before $NaIO_3$ injection, fundus reflectance and AF at both 488-nm and 790-nm channels were nearly homogeneous in all mice.

With SW-AF imaging of *Abca4*$^{-/-}$ mice at age 5 to 6 months, mottling of the fundus was faintly visible 3 days after $NaIO_3$ injection, and after 7 days the heterogeneity was pronounced (Fig. 1A); this small-scale gray-level nonuniformity is similar to that frequently observed in *ABCA4*-associated retinal disease in humans.[39] The mottling with 488-nm excitation was quite pronounced and more prominent in *Abca4*$^{-/-}$ mice after 7 days than in wild-type mice. In *Rpe65*^{rd12} mice that do not accumulate lipofuscin, SW-AF was negligible, $NaIO_3$-associated mottling was not visible, and the images had a uniformly homogeneous appearance. Although the SW-AF images of the *Abca4*$^{-/-}$ and wild-type mice may appear to exhibit similar GLs (Fig. 1A), the internal AF reference (rectangle at top of image) is darker in *Abca4*$^{-/-}$ mice, reflecting the more limited exposure needed to image the higher fundus SW-AF levels in these mice.

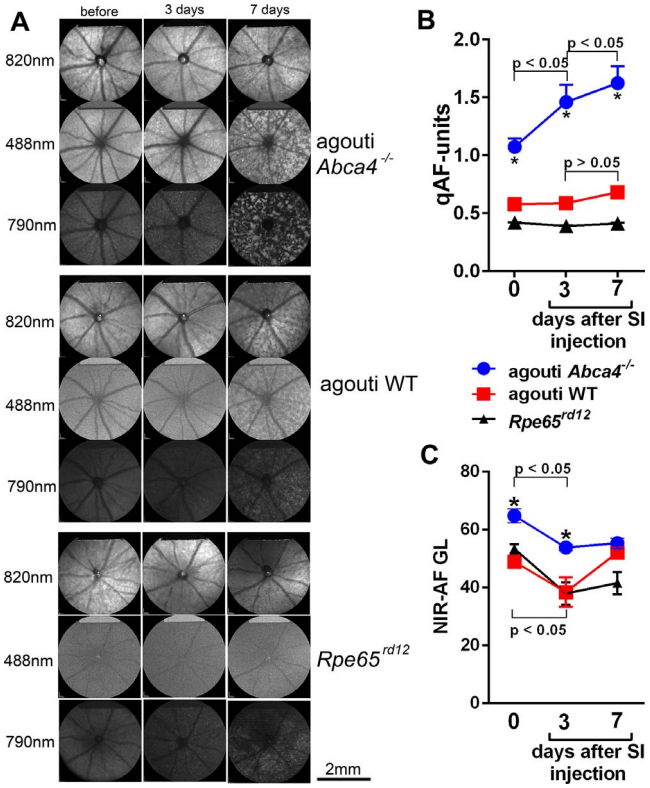

Figure 1. Fundus AF and reflectance imaging of $NaIO_3$-treated mice. (**A**) Fundus images acquired from agouti *Abca4*$^{-/-}$, agouti wild-type (WT), and *Rpe65*^{rd12} mice before and 3 and 7 days after $NaIO_3$ (30 mg/kg) injection: 820-nm, NIR-R; 488-nm, SW-AF; 790-nm, NIR-AF. (**B**) qAF (488 nm) in mice (age 5–6 months). qAF units are calculated as described in the Methods section. Mean ± SEM based on 6 to 7 eyes. (**C**) Measurements of NIR-AF as GLs in mice. Statistical analysis by 1-way ANOVA and Tukey's multiple comparison test. *$P < 0.05$ as compared with WT mice at corresponding time points.

Disuniformity in the NIR-AF images was suggestive of changes in the melanin-containing RPE (Fig. 1A). Good correspondence between SW-AF and NIR-AF patterns was observed (Fig. 1A; 488 and 790 nm). Thus, darkened foci in SW-AF images colocalized with areas of markedly decreased AF in NIR-AF images acquired from *Abca4*$^{-/-}$ mice 7 days after $NaIO_3$ injection. The bright areas of mottling in the NIR-AF images also corresponded to brightness in the SW-AF. The affected versus nonaffected areas of retina were easier to delineate in the NIR-AF images due to greater contrast. These changes in the NIR-AF images were more marked in *Abca4*$^{-/-}$ mice than in wild-type and *Rpe65*^{rd12} mice. Seven days after $NaIO_3$ injection in *Rpe65*^{rd12} mice, areas of aberrant increased and decreased AF signal were visible in the NIR-AF images, probably indicating loss and clumping of RPE cells, respectively.

There were no obvious contrast changes in NIR-R (820 nm) images (Fig. 1A). Given that the signal arises from deeper layers in the NIR-R images, choroidal vessels were occasionally visible.

Quantitative Fundus AF

SW-AF intensities were measured as qAF before $NaIO_3$ (30 mg/kg) injection, 3 days after the injection, and 7 days after the injections (Fig. 1B). As reported previously,[33] qAF intensities were more pronounced in *Abca4*$^{-/-}$ mice than in *Abca4* wild-type mice at the same age. The more robust qAF

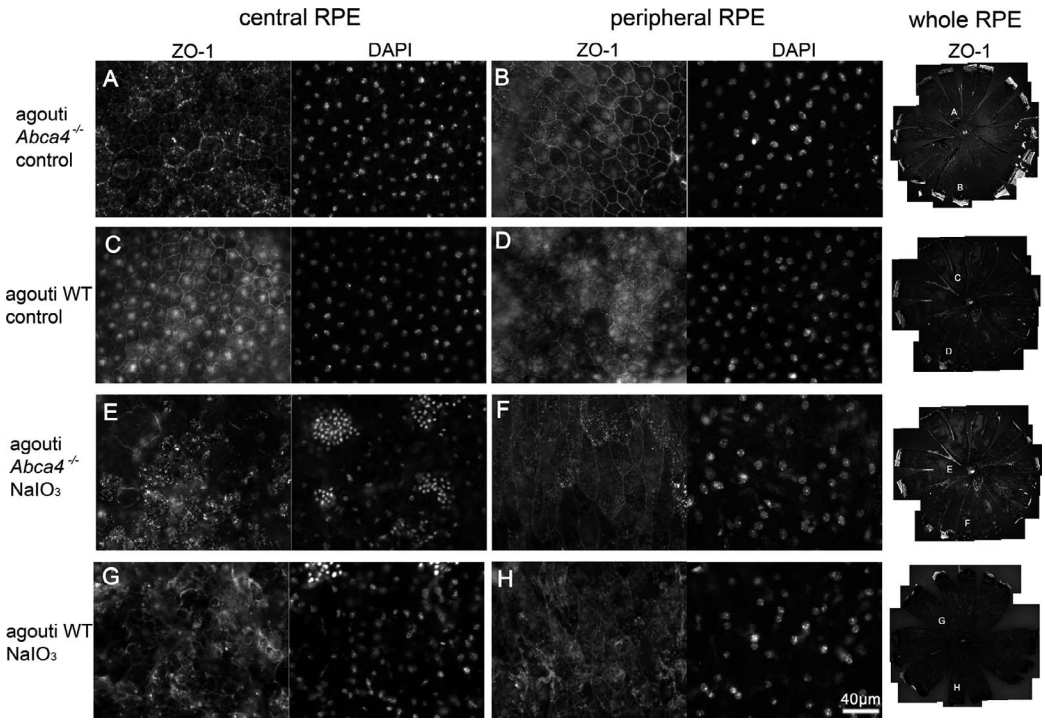

Figure 2. Images acquired from central (**A**, **C**, **E**, **G**) and peripheral (**B**, **D**, **F**, **H**) areas of posterior eyecup flat-mounts with RPE uppermost. Flat-mounts were prepared 7 days after $NaIO_3$ injection. RPE were immunostained with antibody to tight-junction protein ZO-1 and with DAPI to label nuclei. Uninjected agouti *Abca4*$^{-/-}$ (control), uninjected agouti WT (control), agouti *Abca4*$^{-/-}$ injected with sodium iodate ($NaIO_3$), agouti WT injected with $NaIO_3$. Photomontages showing the entire RPE flat-mounts (whole RPE) also are presented.

intensity in *Abca4*$^{-/-}$ mice reflects the well-known accelerated accumulation of bisretinoid lipofuscin as a result of ABCA4 deficiency.[28,40] In *Abca4*$^{-/-}$ mice (age 5–6 months) treated with $NaIO_3$ at 30 mg/kg, SW-AF intensity was increased 3 and 7 days after injection ($P < 0.05$; 1-way ANOVA and Tukey's multiple comparison test). Although in wild-type mice there was a small increase in qAF between 3 and 7 days after injection, this difference was not statistically significant ($P > 0.05$) (Fig. 1B). As expected, minimal SW-AF signal was recorded in *Rpe65*^{rd12} mice due to a paucity of bisretinoid lipofuscin formation.[29,30]

In all three mouse lines (*Abca4*$^{-/-}$, wild-type, and *Rpe65*^{rd12}) NIR-AF measured with 790-nm excitation, was reduced 3 days after $NaIO_3$ injection (Fig. 1C). In agouti *Abca4*$^{-/-}$ and *Rpe65*^{rd12} mice, NIR-AF levels 7 days after injection were at the same level as observed 3 days' postinjection, whereas in wild-type mice, NIR-AF intensity underwent an increase between 3 and 7 days postinjection.

Flat-Mounts

Flat-mounts consisting of RPE, choroid, and sclera were stained with antibody to ZO-1, a protein component of tight junctions, together with nuclear staining by DAPI. In flat-mounts from uninjected eyes of wild-type mice (age 6 months, 2 mice each), the RPE monolayer presented as a regularly arranged cobblestone-like arrangement of hexagonal-shaped cells of similar size (Fig. 2). The DAPI-stained nuclei were relatively uniformly distributed. The posterior eyecups of *Abca4*$^{-/-}$ mice also exhibited positive ZO-1 staining of polygonal-shaped RPE, although in this case the staining was punctate. In addition, the SW-AF of lipofuscin was visible. In eyes of the $NaIO_3$-treated *Abca4*$^{-/-}$ and wild-type mice, the regular cellular mosaic was lost, patchy loss of cells was readily visible, and a granular AF was notable. Large patches of the RPE monolayer were denuded of cells in retinas from $NaIO_3$-treated mice. The regularity of ZO-1 staining was largely disrupted in the *Abca4*$^{-/-}$ and wild-type $NaIO_3$-injected mice after 7 days, and clumps of densely packed nuclei were visible. RPE cells in the periphery appeared elongated. Unexplained nonspecific nuclear staining was observed in the ZO-1–labeled preparations. Because similar staining has been noted in the literature,[16,41] nonspecific antibody binding is the likely cause.

Light Microscopic Imaging

The effects of a single systemic injection of $NaIO_3$ were also visible by light microscopy as progressive RPE and photoreceptor cell degeneration in all injected mice (Fig. 3). Although in hematoxylin and eosin–stained sections of control retina (noninjected) the RPE monolayer consisted of a continuous layer of contiguous cells, in $NaIO_3$-treated retina, the RPE was severely altered as revealed by thinning of the RPE monolayer and gaps in the regular distribution of hematoxylin and eosin–stained RPE nuclei. These features were indicative of RPE loss. The changes in melanin pigment distribution indicated that in some locations, RPE appeared to have migrated anteriorly as previously reported,[18] whereas at other sites, aggregations of RPE cells were visible.

Progressive disorganization of photoreceptor outer and inner segments was indicated by loss of alignment of outer and inner segments. Rosette-like rearrangements of photoreceptor cells in outer retina were also observed as reported previously.[15,36] In areas of absent RPE, ONL appears to have collapsed such that photoreceptor cell nuclei came in contact with Bruch's membrane. Thinning of the ONL in $NaIO_3$-treated agouti *Abca4*$^{-/-}$ mice was more pronounced than in treated wild-type mice.

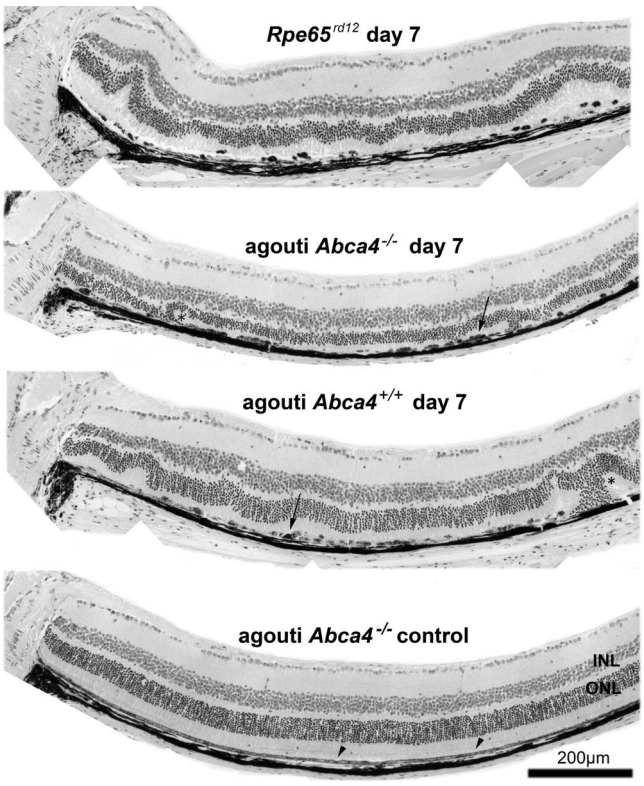

FIGURE 3. Representative light micrographs of superior hemiretina of eyes of *Rpe65*^{rd12}, agouti *Abca4*$^{-/-}$, and agouti *Abca4*$^{+/+}$ mice (age 5–6 months; right or left eyes). Hematoxylin and eosin–stained paraffin-embedded (5 µm) sections at day 7 postinjection of $NaIO_3$. All three treated groups showed changes that included loss of regular spacing and numbers of RPE cell nuclei, clumping of RPE cells (*arrow*) and distortion of outer nuclear and outer segment layers (*). Thinning of the ONL in agouti *Abca4*$^{-/-}$ mice was evident. INL, inner nuclear layer. The ONH is to the far left in all images. RPE, *arrowhead*. *Scale bar*: 200 µm.

Measurement of ONL Thickness

To further assess the effect of $NaIO_3$ on outer neural retina, we evaluated photoreceptor cell viability in *Abca4*$^{-/-}$, wild-type, and *Rpe65*^{rd12} mice by measuring ONL thickness. ONL thickness in 6-month-old agouti *Abca4*$^{-/-}$ mice treated with $NaIO_3$ was reduced versus the nontreated *Abca4*$^{-/-}$ mice and was also lower than in treated wild-type and *Rpe65*^{rd12} mice of the same age (Fig. 4A).

For comparative purposes, we calculated ONL area from the ONH to a distance of 2 mm in a superior and inferior direction (Fig. 4B). ONL area in $NaIO_3$-treated *Abca4*$^{-/-}$ mice was significantly lower than in untreated *Abca4*$^{-/-}$ mice ($P < 0.05$). Of particular interest, the decline in ONL area in $NaIO_3$-treated *Abca4*$^{-/-}$ mice was also significantly lower than in $NaIO_3$-treated wild-type and *Rpe65*^{rd12} mice ($P < 0.05$, 1-way analysis of variance and Tukey's multiple comparison test). It is important to note that $NaIO_3$-induced ONL thinning in 5- to 6-month-old agouti *Abca4*$^{-/-}$ mice (Fig. 4) was accompanied by increased SW-AF (488 nm) (Fig. 1B).

In Vitro Studies

For additional mechanistic studies, we examined $NaIO_3$ activity in vitro (Fig. 5). Delivery of $NaIO_3$ alone to ARPE-19 cells at a concentration of 25 and 250 µM did not cause the death of ARPE-19 cells, but at 2.5 mM approximately 40% loss of viability was observed. On the other hand, intracellular A2E combined with $NaIO_3$ (25 and 250 µM and 2.5 mM in the absence of 488-nm light exposure), was not associated with a further reduction in cell viability (Fig. 5A).

In ARPE-19 cells stressed by A2E accumulation and exposure to 430-nm light, viability was reduced by approximately 38% (Fig. 5A, solid blue bar). This finding is consistent with published results.[35,42] Moreover, this loss of cell viability was exacerbated when the oxidizing environment of the cell was potentiated by a combination of $NaIO_3$ together with the photooxidation of intracellular A2E. Thus, when $NaIO_3$ was delivered to A2E-containing ARPE-19 and the cells were exposed to 430-nm light to induce A2E photooxidation, cell viability was reduced by 57% (250 µM $NaIO_3$) and 64% (2.5 µM $NaIO_3$) ($P < 0.0001$, 1-way ANOVA and Tukey's multiple comparison test). Conversely, when the loss of A2E due to photooxidation was measured chromatographically, we found no evidence that $NaIO_3$ could potentiate the photooxidation of A2E in a cell-free environment, even at the high concentration of 500 µM (Fig. 5B), nor did $NaIO_3$ (100 and 200 µM) alone directly oxidize A2E in a cell-free environment in the absence

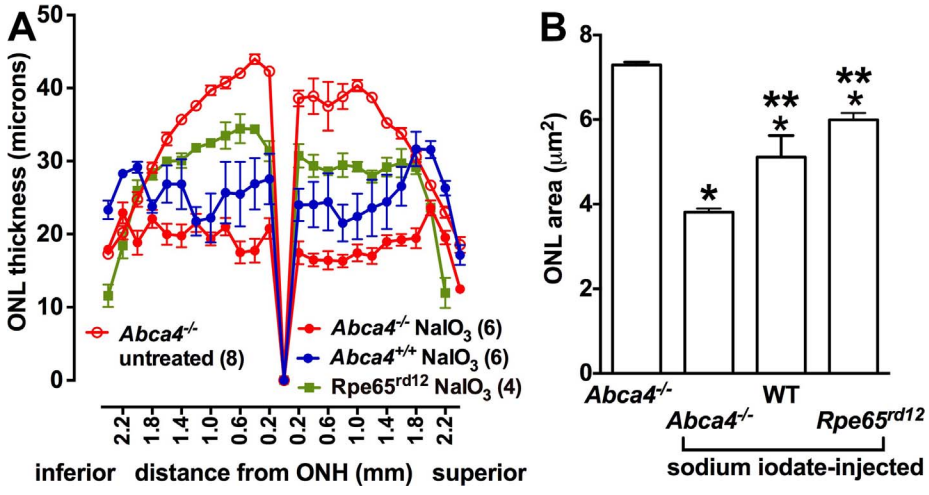

FIGURE 4. ONL thickness measured in $NaIO_3$-treated and untreated *Abca4*$^{-/-}$, *Abca4*$^{+/+}$, and *Rpe65*^{rd12} mice (age 5–6 months). (**A**) ONL thickness is plotted as a function of distance from the ONH. Values are mean ± SEM of numbers of eyes indicated in parentheses. (**B**) Area of ONL calculated from thickness 2-mm superior and inferior to the ONH. *$P < 0.05$ as compared with uninjected control *Abca4*$^{-/-}$ mice; **$P < 0.05$ as compared with sodium iodate–injected *Abca4*$^{-/-}$ mice.

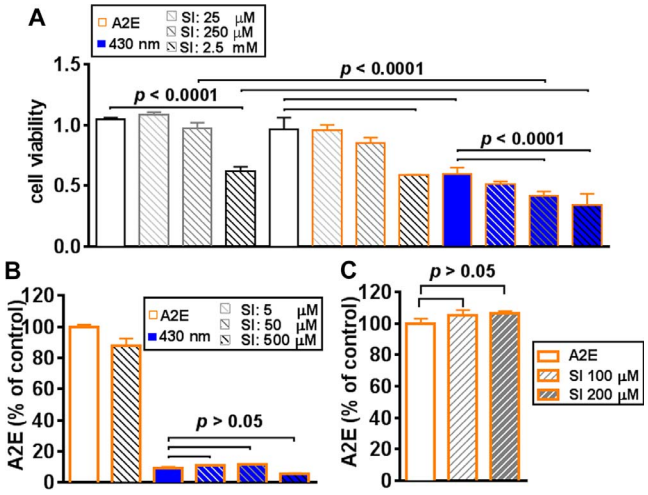

FIGURE 5. In vitro assays of $NaIO_3$ (SI). (**A**) SI at indicated concentrations was incubated with ARPE-19 cells that had not or had accumulated A2E (*bars* outlined in *orange*) and were exposed or not exposed to 430-nm (±30 nm) (*blue bars*) light for 20 minutes. Viability was determined by MTT absorbance (570 nm). Mean ± SEM of six replicates. *P* values determined by 1-way ANOVA and Tukey's multiple comparison test. (**B**) In a cell-free assay, SI at indicated concentrations was combined with A2E (50 μM; *bars* outlined in *orange*) and was or was not (control) exposed to 430-nm light (60 seconds; *blue bars*). A2E photooxidation was assayed by UPLC measurement of A2E loss. SI does not potentiate the photooxidation of A2E. Mean ± SEM of two replicates. $P > 0.05$, 1-way ANOVA, and Tukey's multiple comparison test. (**C**) In a cell-free assay, incubation of A2E (50 μM; *bars* outlined in *orange*) with SI at indicated concentrations for 4 hours does not result in oxidative loss of A2E measured by UPLC. Mean ± SEM of two replicates. $P > 0.05$, 1-way ANOVA, and Tukey's multiple comparison test.

of 488-nm exposure (Fig. 5C). These results indicate that rather than there being molecular interactions between A2E and $NaIO_3$, the combined effects of bisretinoid photooxidative stress and $NaIO_3$ are likely realized as a compromise of cellular oxidant defense.

DISCUSSION

As with genetic ablation of RPE[43] that results in secondary degeneration of photoreceptor cells, $NaIO_3$-induced retinal degeneration begins with RPE cell dysfunction and loss. Indeed, $NaIO_3$-induced retinal degeneration is considered by some investigators to replicate the stages of degeneration observed in atrophic AMD.[3,44] In an effort to understand the primary vulnerability of RPE to the oxidative stress imposed by systemic delivery of $NaIO_3$,[3–6] we tested the premise that the underlying stress imposed by the photoreactivity of RPE bisretinoids could play a role. Thus, we used mice having elevated levels of bisretinoid lipofuscin (*Abca4*$^{-/-}$ mice), mice having wild-type levels, and mice deficient in bisretinoid lipofuscin (*Rpe65*^{rd12}), and observed that the degenerative changes were most marked in *Abca4*$^{-/-}$ mice. Exploration of mechanisms in cultured RPE revealed that the combination of $NaIO_3$ together with A2E and 430-nm light exposure to create photooxidizing conditions produced an additive effect, whereby levels of cell death were greater than A2E/430 nm alone or $NaIO_3$ alone. Previous reports that light exposure and absence of ocular melanin (albinism)[15,24] promote the effects of $NaIO_3$ injection are consistent with our results indicating that underlying photooxidative stress from bisretinoid lipofuscin increases susceptibility of RPE to $NaIO_3$-associated atrophy. It seems that the additive effects of bisretinoid and $NaIO_3$ are manifest at milder concentrations of $NaIO_3$, whereas at high concentrations, $NaIO_3$ alone can impose damage (Fig. 5A).[45] The combined effects of bisretinoid photoxidative stress and $NaIO_3$ likely compromise cellular oxidant defense. For instance, both sources of stress can reduce intracellular glutathione levels[22,46] and the damage mediated by both $NaIO_3$[16] and bisretinoid photooxidative damage[47] can be ameliorated by chelation of labile iron. The pronounced ONL thinning that we observed is also consistent with the view that RPE cell dysfunctioning leading to photoreceptor cell degeneration can precede overt RPE cell loss.[20]

The fluorescent bisretinoids of RPE lipofuscin that are the source of SW-AF fundus AF undergo nonenzymatic formation in photoreceptor cell outer segments. Due to daily shedding of outer segment membrane, the fluorophores then undergo phagocytic transfer to RPE where they accumulate. Because bisretinoid formation precedes RPE phagocytosis, the latter process is unlikely to be a determinant of the rate of RPE lipofuscin formation. We previously proposed that SW-AF fundus AF intensity does not just signal the status of RPE but can under some circumstances be indicative of the health of photoreceptor cells.[26,27] As a test of our hypothesis, here we analyzed SW-AF intensities in mice undergoing $NaIO_3$-induced photoreceptor cell degeneration. We observed a 36% increase in SW-AF intensity within 3 days after injection of $NaIO_3$ in agouti *Abca4*$^{-/-}$ mice. This abrupt rise in qAF cannot be attributed to the normal age-related increase in SW-AF in mice.[31,48] Instead, because this increase coincided with ONL thinning, which is indicative of declining photoreceptor cell function and survival, elevated fundus AF due to augmented bisretinoid formation in stressed photoreceptor cells could explain these findings. These circumstances are significant. Elevated formation of these toxic photoreactive molecules could further accelerate photoreceptor degeneration.

The effects of $NaIO_3$ that are evident in the SW-AF (488 nm) images of $NaIO_3$-treated *Abca4*$^{-/-}$ mice as compared with *Abca4*$^{+/+}$ mice are not just attributable to the greater SW-AF signal in the mutant mice because even in NIR-AF images presenting signal that primarily originates from melanin, the disruptive effects of $NaIO_3$ were more apparent in the NIR-AF images acquired from *Abca4*$^{-/-}$ mice. Thus, multimodal imaging gives emphasis to the more pronounced effects of $NaIO_3$ in mice having RPE burdened by the oxidative stress imposed by elevated bisretinoid lipofuscin.

Pathways combating the effects of $NaIO_3$ also have been reported. For instance, resveratrol, a dietary polyphenol possessing a range of biological actions, protects RPE from $NaIO_3$ through activation of PPARs (peroxisome proliferator-activated receptors) and upregulation of reduced glutathione.[49] In addition, necrostatin-1, an inhibitor of RIPK1 (receptor-interacting protein kinase-1) has also been shown to rescue RPE from death.[6]

From numerous studies over the years, reports have emerged regarding the impact of $NaIO_3$ on retina.[3–9,11] The work presented here has further advanced our understanding of this model. Using both in vitro and mouse models, interactions between the oxidative effects of $NaIO_3$ on RPE and photooxidative stress imposed by lipofuscin bisretinoid also have been revealed. We conclude that photooxidative stress inflicted by RPE bisretinoid lipofuscin contributes to the disposition of RPE toward $NaIO_3$ toxicity. We also suggest that aberrant SW-AF under some conditions may be a sign of impaired photoreceptor cells. These results may impact the interpretations of SW-AF in some retinal disorders.[26,27]

Acknowledgments

Supported by grants from the National Eye Institute (EY12951 and P30EY019007) and Foundation Fighting Blindness, and a grant from Research to Prevent Blindness to the Department of Ophthalmology, Columbia University.

Disclosure: **J. Zhao**, None; **H.J. Kim**, None; **J.R. Sparrow**, None

References

1. Sorsby A. Experimental pigmentary degeneration of the retina by sodium iodate. *Br J Ophthalmol*. 1941;25:58–62.
2. Noell WK. Experimentally induced toxic effects on structure and function of visual cells and pigment epithelium. *Am J Ophthalmol*. 1953;36:103–116.
3. Zhou P, Kannan R, Spee C, Sreekumar PG, Dou G, Hinton DR. Protection of retina by alphaB crystallin in sodium iodate induced retinal degeneration. *PLoS One*. 2014;9:e98275.
4. Carido M, Zhu Y, Postel K, et al. Characterization of a mouse model with complete RPE loss and its use for RPE cell transplantation. *Invest Ophthalmol Vis Sci*. 2014;55:5431–5444.
5. Franco LM, Zulliger R, Wolf-Schnurrbusch UE, et al. Decreased visual function after patchy loss of retinal pigment epithelium induced by low-dose sodium iodate. *Invest Ophthalmol Vis Sci*. 2009;50:4004–4010.
6. Hanus J, Anderson C, Sarraf D, Ma J, Wang S. Retinal pigment epithelial cell necroptosis in response to sodium iodate. *Cell Death Discov*. 2016;2:16054.
7. Kannan R, Hinton DR. Sodium iodate induced retinal degeneration: new insights from an old model. *Neural Regen Res*. 2014;9:2044–2045.
8. Amirpour N, Karamali F, Rabiee F, et al. Differentiation of human embryonic stem cell-derived retinal progenitors into retinal cells by Sonic hedgehog and/or retinal pigmented epithelium and transplantation into the subretinal space of sodium iodate-injected rabbits. *Stem Cells Dev*. 2012;21:42–53.
9. Harris JR, Brown GA, Jorgensen M, et al. Bone marrow-derived cells home to and regenerate retinal pigment epithelium after injury. *Invest Ophthalmol Vis Sci*. 2006;47:2108–2113.
10. Gong LH, Wu Q, Song BW, Lu B, Zhang Y. Differentiation of rat mesenchymal stem cells transplanted into the subretinal space of sodium iodate-injected rats. *Clin Exp Ophthalmol*. 2008;36:666–671.
11. Wang W, Noel J, Kaplan HJ, Dean DC. Circulating reactive oxidant causes apoptosis of retinal pigment epithelium and cone photoreceptors in the mouse central retina. *Ophthalmol Eye Dis*. 2011;3:45–54.
12. Machalinska A, Lubinski W, Klos P, et al. Sodium iodate selectively injuries the posterior pole of the retina in a dose-dependent manner: morphological and electrophysiological study. *Neurochem Res*. 2010;35:1819–1827.
13. Sachdeva MM, Cano M, Handa JT. Nrf2 signaling is impaired in the aging RPE given an oxidative insult. *Exp Eye Res*. 2014;119:111–114.
14. Xia H, Krebs MP, Kaushal S, Scott EW. Enhanced retinal pigment epithelium regeneration after injury in MRL/MpJ mice. *Exp Eye Res*. 2011;93:862–872.
15. Redfern WS, Storey S, Tse K, et al. Evaluation of a convenient method of assessing rodent visual function in safety pharmacology studies: effects of sodium iodate on visual acuity and retinal morphology in albino and pigmented rats and mice. *J Pharmacol Toxicol Methods*. 2011;63:102–114.
16. Hadziahmetovic M, Pajic M, Grieco S, et al. The oral iron chelator deferiprone protects against retinal degeneration induced through diverse mechanisms. *Trans Vis Sci Tech*. 2012;1(3):2.
17. Balmer J, Zulliger R, Roberti S, Enzmann V. Retinal cell death caused by sodium iodate involves multiple caspase-dependent and caspase-independent cell-death pathways. *Int J Mol Sci*. 2015;16:15086–15103.
18. Wang JM, Iacovelli J, Spencer C, Saint-Geniez M. Direct effect of sodium iodate on neurosensory retina. *Invest Ophthalmol Vis Sci*. 2014;55:1941–1952.
19. Kiuchi K, Yoshizawa K, Shikata N, Moriguchi K, Tsubura A. Morphologic characteristics of retinal degeneration induced by sodium iodate in mice. *Curr Eye Res*. 2002;25:373–379.
20. Zhao C, Vollrath D. mTOR pathway activation in age-related retinal disease. *Aging (Albany NY)*. 2011;3:346–347.
21. Hird FJ, Yates JR. The oxidation of protein thiol groups by iodate, bromate and persulphate. *Biochem J*. 1961;80:612–616.
22. Heike M, Marmor MF. L-cystein protects the pigment-epithelium from acute sodium iodate toxicity. *Doc Ophthalmol*. 1990;75:15–22.
23. Toler SM. Oxidative stress plays an important role in the pathogenesis of drug-induced retinopathy. *Exp Biol Med (Maywood)*. 2004;229:607–615.
24. Ikeda H, Adachi-Usami E, Saeki M, Takeda N, Kimura T. Electrophysiological studies on light damage in the mouse retina after sodium iodate injection. *Ophthalmologica*. 1994;208:220–225.
25. Sparrow JR, Gregory-Roberts E, Yamamoto K, et al. The bisretinoids of retinal pigment epithelium. *Prog Retin Eye Res*. 2012;31:121–135.
26. Gelman R, Chen R, Blonska A, Barile G, Sparrow JR. Fundus autofluorescence imaging in a patient with rapidly developing scotoma. *Retin Cases Brief Rep*. 2012;6:345–348.
27. Sparrow JR, Marsiglia M, Allikmets R, et al. Flecks in recessive Stargardt disease: short-wavelength autofluorescence, near-infrared autofluorescence, and optical coherence tomography. *Invest Ophthalmol Vis Sci*. 2015;56:5029–5039.
28. Kim SR, Fishkin N, Kong J, Nakanishi K, Allikmets R, Sparrow JR. The Rpe65 Leu450Met variant is associated with reduced levels of the RPE lipofuscin fluorophores A2E and iso-A2E. *Proc Natl Acad Sci U S A*. 2004;101:11668–11672.
29. Katz ML, Redmond TM. Effect of Rpe65 knockout on accumulation of lipofuscin fluorophores in the retinal pigment epithelium. *Invest Ophthalmol Vis Sci*. 2001;42:3023–3030.
30. Sparrow JR, Kim SR, Jang YP, Zhou J. The lipofuscin of retinal pigment epithelial cells: Learning from mouse models of retinal disease. In: Chalupa LM, ed. *Eye, Retina, and Visual System of the Mouse*. Cambridge, MA: MIT Press; 2008:539–546.
31. Sparrow JR, Blonska A, Flynn E, et al. Quantitative fundus autofluorescence in mice: correlation with HPLC quantitation of RPE lipofuscin and measurement of retina outer nuclear layer thickness. *Invest Ophthalmol Vis Sci*. 2013;54:2812–2820.
32. Delori FC, Greenberg JP, Woods RL, et al. Quantitative measurements of autofluorescence with the scanning laser ophthalmoscope. *Invest Ophthalmol Vis Sci*. 2011;52:9379–9390.
33. Sparrow JR, Blonska A, Flynn E, et al. Quantitative fundus autofluorescence in mice: correlation with HPLC quantitation of RPE lipofuscin and measurement of retina outer nuclear layer thickness. *Invest Ophthalmol Vis Sci*. 2013;54:2812–2820.
34. Parish CA, Hashimoto M, Nakanishi K, Dillon J, Sparrow JR. Isolation and one-step preparation of A2E and iso-A2E, fluorophores from human retinal pigment epithelium. *Proc Natl Acad Sci U S A*. 1998;95:14609–14613.

35. Sparrow JR, Zhou J, Ben-Shabat S, Vollmer H, Itagaki Y, Nakanishi K. Involvement of oxidative mechanisms in blue-light-induced damage to A2E-laden RPE. *Invest Ophthalmol Vis Sci*. 2002;43:1222–1227.
36. Yang YP, Ng TK, Ye C, et al. Assessing sodium iodate-induced outer retinal changes in rats using confocal scanning laser ophthalmoscopy and optical coherence tomography. *Invest Ophthalmol Vis Sci*. 2014;55:1696–1705.
37. Delori FC, Dorey CK, Staurenghi G, Arend O, Goger DG, Weiter JJ. In vivo fluorescence of the ocular fundus exhibits retinal pigment epithelium lipofuscin characteristics. *Invest Ophthalmol Vis Sci*. 1995;36:718–729.
38. Keilhauer CN, Delori FC. Near-infrared autofluorescence imaging of the fundus: visualization of ocular melanin. *Invest Ophthalmol Vis Sci*. 2006;47:3556–3564.
39. Burke TR, Duncker T, Woods RL, et al. Quantitative fundus autofluorescence in recessive Stargardt disease. *Invest Ophthalmol Vis Sci*. 2014;55:2841–2852.
40. Mata NL, Weng J, Travis GH. Biosynthesis of a major lipofuscin fluorophore in mice and humans with ABCR-mediated retinal and macular degeneration. *Proc Natl Acad Sci U S A*. 2000;97:7154–7159.
41. Izawa H, Inoue Y, Ohno Y, et al. Protective effects of antiplacental growth factor antibody against light-induced retinal damage in mice. *Invest Ophthalmol Vis Sci*. 2015;56:6914–6924.
42. Sparrow JR, Nakanishi K, Parish CA. The lipofuscin fluorophore A2E mediates blue light-induced damage to retinal pigmented epithelial cells. *Invest Ophthalmol Vis Sci*. 2000;41:1981–1989.
43. Longbottom R, Fruttiger M, Douglas RH, Martinez-Barbera JP, Greenwood J, Moss SE. Genetic ablation of retinal pigment epithelial cells reveals the adaptive response of the epithelium and impact on photoreceptors. *Proc Natl Acad Sci U S A*. 2009;106:18728–18733.
44. Enzmann V, Row BW, Yamauchi Y, et al. Behavioral and anatomical abnormalities in a sodium iodate-induced model of retinal pigment epithelium degeneration. *Exp Eye Res*. 2006;82:441–448.
45. Juel HB, Faber C, Svendsen SG, Vallejo AN, Nissen MH. Inflammatory cytokines protect retinal pigment epithelial cells from oxidative stress-induced death. *PLoS One*. 2013;8:e64619.
46. Yoon KD, Yamamoto K, Zhou J, Sparrow JR. Photo-products of retinal pigment epithelial bisretinoids react with cellular thiols. *Mol Vis*. 2011;17:1839–1849.
47. Lukinova N, Iacovelli J, Dentchev T, et al. Iron chelation protects the retinal pigment epithelial cell line ARPE-19 against cell death triggered by diverse stimuli. *Invest Ophthalmol Vis Sci*. 2009;50:1440–1447.
48. Flynn E, Ueda K, Auran E, Sullivan JM, Sparrow JR. Fundus autofluorescence and photoreceptor cell rosettes in mouse models. *Invest Ophthalmol Vis Sci*. 2014;55:5643–5652.
49. Qin SF, Lu YM, Rodrigues GA. Resveratrol protects RPE cells from sodium iodate by modulating PPAR alpha and PPAR delta. *Exp Eye Res*. 2014;118:100–108.

Investigative Ophthalmology & Visual Science